Chemistry Faculty Publications   Chemistry

5-27-2005

An investigation of the chemistry of ship emission plumes during ITCT 2002

G. Chen
NASA Langley Research Center

L. G. Huey
Georgia Institute of Technology

M. Trainer
National Oceanic and Atmospheric Administration

D. Nicks
Ball Aerospace

J. Corbett
University of Delaware

See next page for additional authors

Follow this and additional works at: https://scholars.fhsu.edu/chemistry_facpubs

Part of the Chemistry Commons

Recommended Citation

Authors

G. Chen, L. G. Huey, M. Trainer, D. Nicks, J. Corbett, T. Ryerson, D. Parrish, J. A. Neuman, J. Nowak, D. Tanner, J. Holloway, C. Brock, J. Crawford, J. R. Olson, A. Sullivan, R. Weber, S. Schauffler, S. Donnelly, E. Atlas, J. Roberts, F. Flocke, G. Hübler, and F. Fehsenfeld

An investigation of the chemistry of ship emission plumes during ITCT 2002

G. Chen,[1] L. G. Huey,[2] M. Trainer,[3] D. Nicks,[4] J. Corbett,[5] T. Ryerson,[3] D. Parrish,[3] J. A. Neuman,[6,7] J. Nowak,[6,7] D. Tanner,[2] J. Holloway,[6,7] C. Brock,[6,7] J. Crawford,[1] J. R. Olson,[1] A. Sullivan,[2] R. Weber,[2] S. Schauffler,[8] S. Donnelly,[8,9] E. Atlas,[8,10] J. Roberts,[3] F. Flocke,[8] G. Hübler,[6,7] and F. Fehsenfeld[3,11]

[1] A ship emission plume experiment was conducted about 100 km off the California coast during the NOAA Intercontinental Transport and Chemical Transformation (ITCT) 2K2 airborne field campaign. Measurements of chemical species were made from the NOAA WP-3D aircraft in eight consecutive transects of a ship plume around midday during 2.5 hours of flight. The measured species include NO_x, HNO_3, peroxyacetylnitrate (PAN), SO_2, H_2SO_4, O_3, CO, CO_2, nonmethane hydrocarbons (NMHC), and particle number and size distributions. Observations demonstrate a NO_x lifetime of ~1.8 hours inside the ship plume compared to ~6.5 hours (at noontime) in the moderately polluted background marine boundary layer of the experiment. This confirms the earlier hypothesis of highly enhanced in-plume NO_x destruction. Consequently, one would expect the impact of ship emissions is much less severe than those predicted by global models that do not include rapid NO_x destruction. Photochemical model calculations suggest that more than 80% of the NO_x loss was due to the NO_2 + OH reaction; the remainder was by PAN formation. The model underestimated in-plume NO_x loss rate by about 30%. In addition, a comparison of measured to predicted H_2SO_4 in the plumes suggests that the photochemical model predicts OH variability reasonably well but may underestimate actual values. Predictions of in-plume O_3 production agree well with the observations, suggesting that model-predicted peroxy radical (HO_2 + RO_2) levels are reasonable. The model estimated ozone production efficiency ranges from 6 to 30. The largest model bias was seen in the comparison with measured HNO_3. The model overestimated in-plume HNO_3 by about a factor of 6. This is most likely caused by underestimated HNO_3 sinks possibly involving particle scavenging. However, limited data availability precluded a conclusive test of this possible loss process.

1. Introduction

[2] Emissions from oceangoing ships have increasingly become a concern in terms of their impact on climate and the chemistry of the marine atmosphere [e.g., *Corbett*, 2003; *Corbett and Koehler*, 2003; *Sinha et al.*, 2003; *Durkee et al.*, 2000a]. *Beirle et al.* [2004] recently detected elevated NO2 levels along congested ship traffic near Sri Lanka from satellite observations. On the basis of 1990s fuel consumption estimates, recent studies have placed ship emissions of NO_x (NO + NO_2) and SO_2 at 2.8–3.5 TgN yr^{-1} and 2.5–4.2 TgS yr^{-1}, respectively [e.g., *Endresen et al.*, 2003; *Skjølsvik et al.*, 2000; *Corbett et al.*, 1999]. The center of the NO_x range represents 14% of the total global emissions from fossil fuel combustion estimated by *Lee et al.* [1997].

[1]NASA Langley Research Center, Hampton, Virginia, USA.
[2]School of Earth and Atmospheric Sciences, Georgia Institute of Technology, Atlanta, Georgia, USA.
[3]Aeronomy Laboratory, National Oceanic and Atmospheric Administration, Boulder, Colorado, USA.
[4]Ball Aerospace, Boulder, Colorado, USA.
[5]Marine Policy Program, Graduate College of Marine Studies, University of Delaware, Newark, Delaware, USA.
[6]Cooperative Institute for Research in Environmental Sciences, University of Colorado, Boulder, Colorado, USA.

[7]Also at Aeronomy Laboratory, National Oceanic and Atmospheric Administration, Boulder, Colorado, USA.
[8]Atmospheric Chemistry Division, National Center for Atmospheric Research, Boulder, Colorado, USA.
[9]Now at Department of Chemistry, Fort Hays State University, Hays, Kansas, USA.
[10]Now at Division of Marine and Atmospheric Chemistry, Rosenstiel School of Marine and Atmospheric Science, University of Miami, Miami, Florida, USA.
[11]Also at Cooperative Institute for Research in Environmental Sciences, University of Colorado, Boulder, Colorado, USA.

Though ship emissions of sulfur are only 4% of total fossil fuel sulfur emissions, they are comparable to current estimates of natural oceanic dimethylsulfide (DMS) emissions in many remote marine regions of the Northern Hemisphere and in some regions of the Southern Hemisphere [*Corbett et al.*, 1999]. Furthermore, studies using the updated fuel consumption data for 2001 report nearly double the emissions cited in previous works [*Corbett*, 2003; *Corbett and Koehler*, 2003; *Corbett et al.*, 1999]. Emissions of aerosol particles, including black carbon and CCN, have recently been documented by *Sinha et al.* [2003] and *Hobbs et al.* [2000]. These emissions can increase the concentration of cloud droplets and lead to enhancement in the albedo of marine stratiform clouds [e.g., *Twomey*, 1977; *Radke et al.*, 1989; *Ferek et al.*, 1998], which may enhance the radiative cooling effect. The Monterey Area Ship Track Experiment (MAST) has advanced our understanding of the mechanisms by which ship emissions can influence the optical properties and the formation of marine boundary layer clouds [e.g., *Durkee et al.*, 2000b; *Hobbs et al.*, 2000; *Noone et al.*, 2000].

[3] Several theoretical studies have evaluated the chemical and climate impact of ship emissions with global models. *Capaldo et al.* [1999] suggested that ship emissions are a dominant source of SO_2 over much of the world's ocean and may produce a significant fraction of NSS (non-sea-salt) sulfate aerosol in these areas. These authors also estimated CCN (cloud condensation nuclei) emission rates and predicted a shift of -0.11 Wm^{-2} in global radiative forcing due to ship emitted particulate matter. Conversely, *Endresen et al.* [2003] concluded that the overall effect of ship emissions on radiative forcing is small due to canceling effects. *Lawrence and Crutzen* [1999] focused their effort on the effect of ship NO_x emissions. Their chemical transport model (CTM) predictions showed significantly higher marine boundary layer NO_x levels than those omitting ship emissions. In heavily trafficked shipping lanes the predicted enhancements were over 100 fold. Consequently, these NO_x increases would lead to a quite noticeable effect on both surface ozone and OH levels. The estimated ozone enhancement in the central North Atlantic and Pacific was over a factor of 2 and model-predicted OH increases were up to a factor of 5 compared to expected levels if ship emissions were neglected.

[4] *Kasibhatla et al.* [2000] performed a similar modeling study with a more refined emission database and an improved geographical distribution of oceangoing ships but found that the predicted enhancement in NO_x was not supported by observations. Comparison with data from the North Atlantic Regional Experiment (NARE) 1997 revealed that the model consistently over-estimated the observed NO_x levels by up to factor of 10. Even with further refined emission data, the CTM study by *Endresen et al.* [2003] still over-predicted the median boundary layer NARE NO_x level by nearly a factor of 6. Interestingly, even when ship emissions were not considered, the model still over-predicted NO_x by about a factor of 2 for both studies. *Davis et al.* [2001] further compared the global modeling results of *Kasibhatla et al.* [2000] with the data sets generated from 5 NASA Global Tropospheric Experiment (GTE) airborne campaigns from 1991 to 1999 in the North Pacific. This comparison revealed that the predicted NO_x

levels were 3.3 and 5 times higher than the observed values for spring and fall seasons, respectively. Again, the model was found to over-predict NO_x even for the no-ship case.

[5] To reconcile these large differences between measurements and model predictions, several hypotheses have been put forward involving both overestimation of emission inventories and missing plume chemical and dynamical processes. One hypothesis is that CTM simulations do not properly treat the chemistry in ship plumes where NO_x can be oxidized with a lifetime of a few hours. By contrast, the NO_x lifetime is typically estimated to be around 1 day in the marine boundary layer by CTM models [*Kasibhatla et al.*, 2000]. This means that a large fraction of the ship emitted NO_x can be rapidly removed from the boundary layer before it is diluted to the grid size of a CTM. Power plant plume studies have demonstrated shorter in-plume NO_x lifetimes in comparison to those estimated for background conditions [e.g., *Ryerson et al.*, 1998]. By contrast, the lifetime of SO_2 is primarily controlled by heterogeneous processes that are largely independent of plume chemistry. It is interesting to note that CTM-predicted SO_2 levels are only about a factor of 2 lower than observed values [*Davis et al.*, 2001]. Even this difference may be simply due to a bias in emission estimates. The latest global SO_2 emission estimate shows a ~11% increase, which would lead to a modest reduction in the magnitude of the model bias.

[6] Several studies have focused on the impact of detailed ship plume dynamics on the chemistry of the emissions using Lagrangian box models [*von Glasow et al.*, 2003; *Song et al.*, 2003a, *Davis et al.*, 2001]. *Song et al.* [2003a] suggested that the in-plume NO_x lifetime would be a factor of 2.5–10 shorter than in the ambient MBL primarily due to elevated plume OH levels. *von Glasow et al.* [2003] show similar results and suggest that neglecting detailed plume chemistry in a global model overestimates the effect of ship emissions on ozone production by 50% and on OH levels by a factor of 2.

[7] The ship emissions of particles and SO_2 were also examined in box model studies. In particular, *von Glasow et al.* [2003] assessed the impact of aerosol particles on plume chemistry and concluded that the background (sulfate and sea salt) aerosols can have a significant influence on the gas phase chemistry of the ship plume while the ship emitted particles (including soot) had little additional effect. *Song et al.* [2003b] suggested that the major loss of SO_2 is heterogeneous removal and the meteorological stability is the largest factor that controls the plume SO_2 levels. The predicted SO_2 and NSS are at the highest levels under stable conditions when the dilution rate is slower, in comparison with neutral or unstable conditions.

[8] Although modeling studies have shown the potential impact of ship emissions, observations are needed to test these predictions. In fact, several of the theoretical studies have stated the need for experimental data to better elucidate the dynamical and chemical processes of ship plumes [e.g., *Corbett*, 2003; *von Glasow et al.*, 2003, *Davis et al.*, 2001; *Lawrence and Crutzen*, 1999]. Observations of ship plumes can help us better determine the rate of the plume dispersion and also provide the observed NO_x concentration as model constraints to examine various aspects of the plume chemistry.

[9] In this work we report the results of an experimental investigation of ship plumes made during NOAA ITCT (Intercontinental Transport and Chemical Transformation) 2K2 field campaign onboard the WP-3D aircraft on 8 May 2002 off the coast of California. During this flight, many gas phase and aerosol chemical species, aerosol size distributions, and meteorological parameters were measured in successive transects of a ship emission plume. Analysis of these data enables us to assess our understanding of ship plume chemistry, factors controlling NO_x loss, and the chemical interaction between particulate matter (both background and ship emitted) and plume gases.

2. Methods

2.1. Instrumentation

[10] The NOAA WP-3D was equipped with a large suite of instruments to measure gas phase compounds, particle composition, particle size distributions, and meteorological parameters. The aircraft was based out of Monterey, CA during the ITCT 2K2 study. The instrumentation package has been summarized by *Parrish et al.* [2004], *Brock et al.* [2003], and *Nowak et al.* [2004]. The measurements relevant to this study include NO, NO_2, NO_y, O_3, CO, CO_2, NMHCs (nonmethane hydrocarbons), SO_2, HNO_3, H_2SO_4, as well as aerosol size distributions and chemical composition. Most of the individual instruments have been deployed previously on the NOAA aircraft and are described in detail elsewhere [*Brock et al.*, 2000, 2003, *Ryerson et al.*, 1998; *Holloway et al.*, 2000; *Ryerson et al.*, 2001; *Neuman et al.*, 2002; *Heidt et al.*, 1989; *Schauffler et al.*, 1999; *Nicks et al.*, 2003]. The measurements of gas phase sulfuric acid (H_2SO_4), and particle composition were added to the WP-3D payload for the ITCT mission. H_2SO_4 was measured once every two seconds with a chemical ionization mass spectrometer (CIMS) mounted in a pod underneath the port wing of the aircraft. The CIMS instrument and sampling inlet were based on the methods of Eisele and coworkers [*Eisele and Tanner*, 1993; *Eisele et al.*, 1997; *Mauldin et al.*, 1999a, 1999b]. Particle composition was measured once every 4 min with a particle-into-liquid sampler (PILS) coupled to an ion chromatograph [*Weber et al.*, 2001; *Orsini et al.*, 2003]. The aircraft was also equipped with a new low turbulence inlet (LTI) that allowed efficient sampling of larger particles [*Brock et al.*, 2003, 2004; *Wilson et al.*, 2004]. Both the aerosol sizing and composition instruments sampled from the LTI.

2.2. Model

[11] A photochemical box model is used here primarily to provide estimates of short-lived compounds such as OH and H_2SO_4. The model contains explicit HO_x-NO_x-CH_4 chemistry and parameterized NMHC chemistry; it has been used extensively in other airborne studies [*Davis et al.*, 1996; *Crawford et al.*, 1999; *Chen et al.*, 2000; *Olson et al.*, 2001]. The NMHC chemical mechanism is a modified version of the condensed mechanism of *Lurmann et al.* [1986] to accommodate low NO_x conditions (e.g., organic peroxide formation and feedbacks) and to represent explicit chemistry of acetone, propane, and benzene. A detailed listing of reactions can be found in the Appendix of *Crawford et al.* [1999]. The rate coefficients for gas phase reactions are those recommended by *DeMore et al.* [1997]. The photolysis rate coefficients, j values, were calculated for clear-sky conditions using a DISORT (discrete ordinates radiative transfer) four-stream implementation of the NCAR TUV (Tropospheric Ultraviolet Visible) radiative transfer model. The total ozone column data used in the TUV calculations was taken from satellite observations (http://toms.gsfc.nasa.gov/ozone/ozone.html). On the basis of visual observations and photographs taken during the flight, clear sky conditions were deemed appropriate for the radiative calculations. Rigorous ground based comparison has shown that TUV predicted $j(NO_2)$ is highly consistent with observations [*Shetter et al.*, 2003].

[12] The model also includes surface and heterogeneous loss processes for soluble species (e.g., HNO_3, H_2SO_4). These loss processes are parameterized as first-order reactions and the loss coefficients are derived from *Logan et al.* [1981]. However, when aerosol number/size distribution data are available, the rate of heterogeneous loss (or aerosol scavenging) is calculated using the formulation cited in the work of *Fuchs and Sutugin* [1970]. The mass accommodation coefficients and/or reaction probabilities were taken from recent literature (see later discussions).

[13] The model input consists of the 1 s observations of NO, CO, O_3, H_2O, SO_2, temperature and pressure, and grab sample observations of NMHC. The high temporal resolution is required for plume analysis because of the small size of the plumes (<20 km) and the high speed (~100 m s^{-1}) of the aircraft. The model output includes OH, HO_2, RO_2 (organic peroxy radicals), H_2SO_4, HNO_3 and rates of photochemical ozone formation and destruction. We opt to use the instantaneous photostationary state solution (dc/dt = 0) for the model output. This type of solution can provide adequate estimates for short-lived species in plume conditions. The same approach was also taken in earlier studies conducted in similar conditions [e.g., *Frost et al.*, 1999, 2002]. Additional sensitivity model runs were carried out to examine the impact of longer lived species (i.e., CH_2O) on model OH estimates. Limited Lagrangian calculations with parameterized dilution terms (see equation (4)) were also conducted to simulate the in-plume evolution of longer lived species (e.g., HNO_3, PAN and O_3). In these cases, the rates of photochemical production and loss were estimated using model calculations constrained by the observations recorded during the 8 plume transects. Interpolated values were used at the times between these transects.

3. Observations

3.1. Sampling Strategy and Background Conditions

[14] The ITCT 2K2 ship plume experiment was conducted around noon on 8 May 2002 about 100 km off the coast of California. Satellite images taken during the MAST study in 1994 demonstrate that this area has heavy ship traffic [*Durkee et al.*, 2000a]. In situ observations of chemical tracers and wind patterns suggest that this region was moderately polluted, probably due to a combination of aged continental air with more recent inputs from the shipping lanes and possibly offshore platforms. This was supported by back trajectories that were essentially parallel to the Pacific coast for several days. The observed median background levels in the marine boundary layer outside of
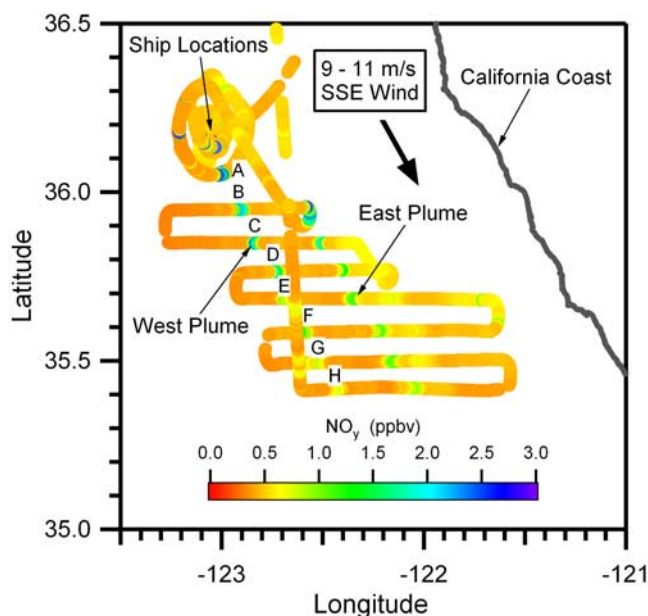
Figure 1. Illustration of the ITCT 2K2 ship plume sampling strategy. The flight track of the WP-3D is color coded by the observed NO_y levels. The wind direction and speed are also indicated. The plume transects are labeled sequentially as A through H.

ship plumes for NO_x, O_3, and CO were ~150 pptv, 40 ppbv, and 130 ppbv, respectively. Modestly elevated NMHC (nonmethane hydrocarbon) levels were also observed, e.g., C_3H_8 ranged from 300–400 pptv with a median of 370 pptv. The corresponding ratios of C_2Cl_4/CO and C_2H_2/CO were estimated to be 0.04 and 1.5 (pptv/ppbv), which are indicative of anthropogenic influences from urban/industrial sources [*Smyth et al.*, 1996; *Blake et al.*, 1999]. Particle number and size distribution measurements give an average total background volume concentration and surface area concentration of 7 μm^3 cm^{-3} and 90 μm^2 cm^{-3}, respectively. In addition, average particulate sulfate and sulfur dioxide levels were 1.0 μg cm^{-3} and 0.5 ppbv, respectively. These levels are much higher than expected in a remote marine boundary layer and are probably due to sulfur rich emissions from ships.

[15] On the day of the ship experiment, visual observations indicated clear sky conditions with a few scattered clouds. The wind direction was consistently between 300°– 325° and the average wind speed was 9–11 m s^{-1}. The height of the marine boundary layer determined from aircraft altitude profiles varied from ~350 m to ~250 m through the sampling period. The observed atmospheric lapse rates suggest the meteorological stability was between neutral and unstable.

[16] Two ship plumes designated as east and west were encountered during the flight. The location of each plume is apparent in the measurements of NO_y color-coded along the flight track of the WP-3D in Figure 1. The orientation of the ship plume is also consistent with the wind direction which is annotated in the figure. In the case of the east plume, there is no known information about the ship location or course. The west plume was a mixture of emissions from two ships close in location. The position, heading, and speed of the

ships were visually determined. Ship 1 was heading WNW and Ship 2 was heading NNW; both at a speed of ~5 m s^{-1} (~9.7 knots). The aircraft sampling height for the plumes was ~100 m above sea level. The initial sampling of the west plume was carried out by circling the ships. The closest sampling of the plumes occurred within 5 km downwind from the ships. The plumes from both ships were individually identified in circular sampling around the ships but merged into one further downwind. The data from the circular samplings were used to obtain emission factors for both ships. The coalesced plume was then systematically intercepted 8 times downwind, identified by the letters A-H as seen in Figure 1, which corresponds to plume ages of up to ~2.5 hours (see discussion in section 3.3). It can be seen in Figure 1 that both plume tracks were essentially straight lines, indicating steady winds. The east plume was also periodically intercepted during the experiment but this data is analyzed at a lower level of detail as the background levels outside of the plume as well as the origin of the plume were less well defined. Discussions later in the text are focused on the west plume, unless specified otherwise. Two points should be noted about the plume sampling. First, two ships with different headings might be expected to form two separate plumes; however, visual observations showed the two ships were in close proximity, which facilitated the merge of their emissions into one plume. This merged plume was then consistently sampled in approximately a Lagrangian manner, i.e., the plane moved downwind at the speed close to that of the plume. Second, the heading of the ships almost directly into the wind, high wind speed, and the neutral to unstable stability conditions are factors all in favor of rapid dilution of the plume. This implies that this study may have been carried out at emission concentrations below typical values for ship plumes.

[17] One of the ships that formed the west plume was later identified as a 26,562 ton bulk carrier. Its diesel engine runs on marine fuel oil and generates ~9120 to 10,730 horse power. The fuel consumption rate at sea is 27 tons day^{-1}. The service speed is 14.5 knots (26.9 km $hour^{-1}$).

3.2. Ship Emission Factors

[18] One major uncertainty in evaluating the impact of ship emissions is the estimate of the emission rates. Direct observations of the ship plumes can be used to estimate the emission factors (i.e., emission of certain species in gram per kilogram fuel consumed) [e.g., *Hobbs et al.*, 2000; *Sinha et al.*, 2003] which are critical parameters in emission inventory studies. For example, *Hobbs et al.* [2000] derived the emission factors for NO_x, SO_2, and particles using the ratio of plume enhancement of effluents to CO_2, e.g., $\Delta NO_x/\Delta CO_2$, $\Delta SO_2/\Delta CO_2$, etc. The emission factors were then calculated based on the mass ratio of CO_2 to marine fuel oil of 3.2. The value of this ratio was derived from works by *Tuttle* [1995] in which the hydrogen atom to carbon atom ratio was found to be 1.8 in marine fuel oil. Similarly, we have derived emission factors for NO_x, SO_2, and aerosol particles based on two plume observations closest to the ships (see Figure 2). The observed values of NO_y, SO_2, CO_2, and total particle concentration, N_{total}, are shown in Figure 2. The ratios of $\Delta NO_x/\Delta CO_2$, $\Delta SO_2/\Delta CO_2$, and $\Delta N_{total}/\Delta CO_2$ were evaluated using the data shown in
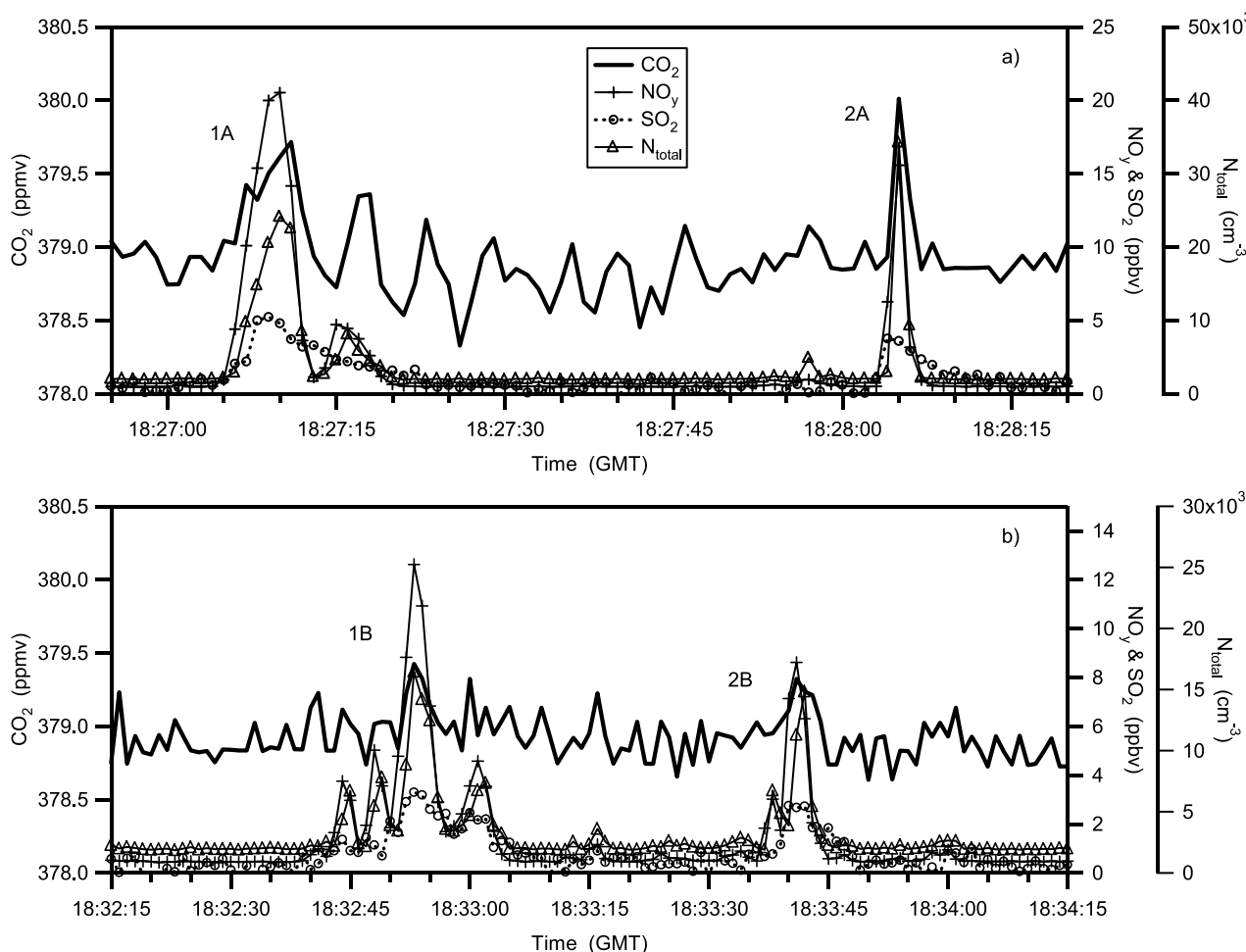
Figure 2. Time series plot of the observed CO_2, NO_y, SO_2, and N_{total} for (a) ship plume transects 1A and 2A as well as (b) 1B and 2B (exact sampling location not shown in Figure 1 because of its scale), which represent the observations closest to the ships. N_{total} represents the total concentration of the particles larger than 5 nm in diameter.

this figure. For the particle emissions the calculation was carried out over two size ranges 0.005–0.15 μm and 0.15–1.0 μm (in diameter). The estimated emission factors are summarized in Table 1 for both ships. The uncertainties quoted in the table reflect both instrument precision and the atmospheric variability in background levels. The latter is especially important in determining the magnitude of the CO_2 enhancement because of the small difference between the plume and background. The estimated NO_x emission factors are consistent with other in situ estimates [e.g., *Hobbs et al.*, 2000; *Sinha et al.*, 2003] and the values commonly used in emission inventory studies [e.g., *Corbett et al.*, 1999]. The total particle emission factors are also consistent with those estimated by *Sinha et al.* [2003]; assuming that N_{total} provides a meaningful comparison point as the measurement size bins are quite different.

[19] The SO_2 emission factors are significantly lower than those estimated for ships burning marine fuel oil [e.g., *Corbett et al.*, 1999; *Corbett and Koehler*, 2003; *Hobbs et al.*, 2000; *Sinha et al.*, 2003]. This may indicate that the sulfur content in the fuel used in the ships observed during ITCT was much lower. Average fuel sulfur contents are about 2.7% for international marine fuels [*Corbett and*

Koehler, 2003; *Endresen et al.*, 2003; *European Commission and ENTEC UK Limited*, 2002; *International Maritime Organization and Marine Environment Protection Committee*, 2001]. Of course, fuel-sulfur levels vary according to when and where fuel is purchased. A recent inventory [*Starcrest Consulting Group LLC et al.*, 2004] of commercial marine vessels in Los Angeles confirmed that average sulfur levels used aboard ships on the west coast of North America is near the world average (averaging 2.64%); interestingly, this inventory also observed some vessels with main engine fuel-sulfur levels at or below 2%. The fuel delivery report obtained for this study indicates that the fuel sulfur content for the identified ship was most likely in the range of 1.9 to 2.2%. It is reasonable to expect that that the other vessel was consuming similar type of fuel. On the basis of the fuel sulfur content values, the SO_2 emission factors are estimated to be 38–44 gSO_2 kg fuel^{-1}, which is still significantly higher than the values listed in Table 1. This discrepancy suggests that the SO_2 emission factors derived from observations are inconsistent with the estimated fuel sulfur content.

[20] We have also investigated whether expected $CO2$ emissions are consistent with the observed plume enhance-

Table 1. Summary of Estimated Emission Factors for Residual Fuel Ships

Species	Ship 1	Ship 2	Typical Range
NO_x (gN/kg fuel)	20 ± 8	13 ± 8	19 ± 8[a]
SO_2 (gSO$_2$/kg fuel)	30 ± 4	23 ± 7	53 ± 7[a]
N_{nucl}[b] (10^{16} particles/kg fuel)	4.6 ± 1.4	4.5 ± 1.8	see *Lyyränen et al.* [1999], *Hobbs et al.* [2000], and *Sinha et al.* [2003]
N_{Pm1c}[c] (10^{14} particles/kg fuel)	2.6 ± 0.8	1.7 ± 1.0	see *Lyyränen et al.* [1999], *Hobbs et al.* [2000], and *Sinha et al.* [2003]
N_{total}[d] (10^{16} particles/kg fuel)	4.6 ± 1.4	4.7 ± 2.3	1.6–6.2,[e] 7 ± 5[a]

[a]Typical ranges estimated from reported average values for various types of vessels [*European Commission and ENTEC UK Limited*, 2002, Tables 2.11–2.13]. Ranges for sulfur are based on heavy fuel oil sulfur contents averaging 2.7% by weight; individual vessels may periodically use fuel with lower sulfur contents than assumed in the ENTEC factors.
[b]N_{nucl} = particles in size range of 0.005–0.15 μm in diameter.
[c]N_{pm1} = particles in size range of 0.15–1 μm in diameter.
[d]N_{tot}: = particles in size range of 0.005–7 μm in diameter.
[e]See *Sinha et al.* [2003] and *Hobbs et al.* [2000].

ments, based on main engine fuel consumption of the identified bulk carrier at 27 ton/day. At the observed ship speed of ∼5 m/s (9.72 knots) and the rated vessel speed of 14.5 knots, engine load was 67% of full speed (∼30% of full power) which translates to a fuel consumption rate of ∼0.3 kg C (carbon)/s. Using the mass ratio of CO_2 emitted to fuel consumed, the CO_2 emission rate would be 1.09 kg/s. A Gaussian plume dispersion model was then used to estimate the CO_2 mixing ratio at 5 km downwind where the ship plume was first spotted. The Gaussian plume dispersion scheme used in the calculation is that described by *Song et al.* [2003a], which is based on the offshore dispersion model developed by *Hanna et al.* [1985]. The model results show a high sensitivity to the meteorological stability. As mentioned earlier, the observed lapse rates suggest conditions were between neutral and unstable. The model-predicted centerline CO_2 plume enhancements for these two conditions were 0.22 and 2.0 ppmv, respectively. This brackets the observed CO_2 enhancement of ∼1 ppmv. Considering the large uncertainties in the dispersion model, it is clear that better models need to be incorporated in ship plume studies to represent the plume dispersion processes under actual ambient conditions.

3.3. Evolution of the Ship Plume

[21] Figures 3a–3c shows three transects of the WP-3D of the west plume labeled west A, C, and H. These plots are time series of 1 second observations of NO_x, SO_2, and N_{total} (total particle number concentration). The width of the sampled plume ranges from five to ten km (∼50 s to ∼100 s of flight time) and requires the use of high resolution data to accurately characterize the plume even though the imprecision is large in some of the 1 second data, particularly for SO_2. In Figures 3a and 3b, significant enhancements can be seen for all these species above background for west A and C. In the case of west H, the plume SO_2 level is indistinguishable from the background; however, the enhancements of NO_x and N_{total} are still evident, especially for N_{total}. The large variations observed during the west A transect suggest that the two plumes were partially mixed. The smaller variations observed in the later plume transects indicate that the plumes have become more thoroughly mixed.

[22] The decay of ship effluents is illustrated in Figure 4 which plots the average plume mixing ratio versus the age of the plume for all 8 transects for NO_x, SO_2, and N_{total}.

Also shown are the corresponding background levels estimated from the data collected 30 s before and after the plume. The plume age is defined as the time elapsed between emission and sampling. Since ship information (i.e., speed, heading, and location) is limited to the initial visual observations, it is difficult to determine the absolute age of the plumes sampled in transect A through H. However, the relative plume age between transects can be readily calculated using the observed wind speed and locations of the plumes. The aircraft position is determined from GPS coordinates. Therefore the estimated relative plume ages are reasonably precise, although the absolute age may have a significant offset. The plume age for transect A shown on the plots was estimated as the time required for the plume to travel from the location where ships were initially spotted by NOAA WP-3D.

[23] A data filter is used to compute the averages displayed in Figure 4. This filter is based on total particle concentration, N_{total}. N_{total} is expected to experience changes due only to dilution. Particle loss through dry deposition and coagulation are estimated to be negligible. In addition, the observation of ultrafine particle (5–10 nm) suggests the maximum nucleation effect on N_{total} to be less than 3% for west A and this effect will rapidly decrease for the later transects. For a given transect (e.g., west A), the filtered averages contain only the data points for which the concurrent in-plume N_{total} enhancement (plume value minus background) is higher than 50% of the peak value. The peak value is defined as the 90th percentile of a given transect. The purpose of this filter is to better represent the center plume levels of the variables of interest.

[24] As shown in Figure 4, the average plume concentrations of the ship effluents decrease as the plume ages. The magnitude of the decrease in the plume enhancement is different for each of these three species. The observed decreases can be explained by plume dispersion and other losses including chemical conversion, particle scavenging, and surface deposition. Since the losses (i.e., deposition and coagulation) and production (i.e., nucleation) of N_{total} are negligible, the rate of dispersion can be derived by assessing the rate of decay of ΔN_{total} (plume average minus background) with respect to time. Assuming a constant background, a dispersion lifetime of ∼2.5 ± 0.6 hours is determined by a least squares regression analysis weighted by the relative uncertainties estimated for ΔN_{total}. The R^2 value is estimated at 0.78.
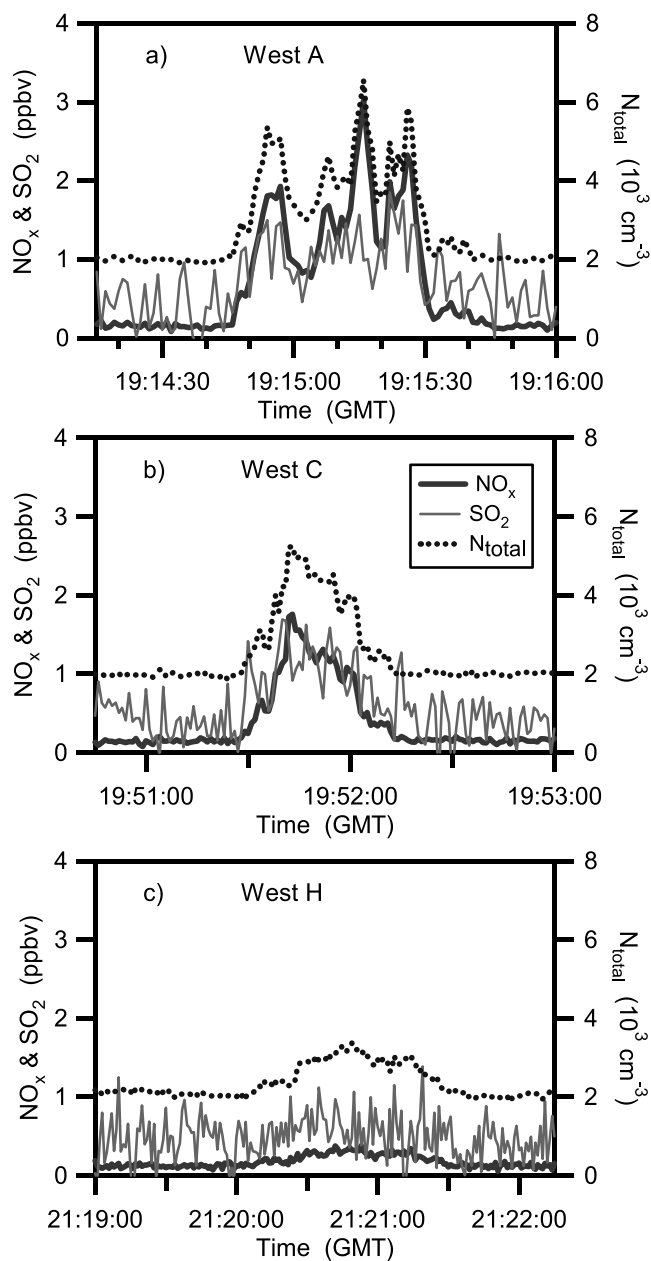
Figure 3. Time series of observed NO_x (solid line), SO_2 (dotted line), and N_{total} (dashed line) for ship plume transects (a) A, (b) C, and (c) H. N_{tot} represents the total concentration of the particles. Note that the SO_2 data represent 5-s averages.

[25] For the case of NO_x, there are significant additional losses due to photochemical processes. The first-order loss rate coefficient k_{NOx} for all photochemical losses can be estimated using the concentration ratio approach as described by *Ryerson et al.* [1998], i.e.,

$$\frac{\Delta NO_x}{\Delta N_{total}} = \exp\left(-k_{NOx}t_p\right) \quad (1)$$

where ΔNO_x is the NO_x enhancement due to ship emission above background, ΔN_{total} is the plume enhancement in N_{total}; and t_p is plume age. By contrast, this method is not suitable to estimate SO_2 lifetime. As shown in Figure 4b, 6

out of 8 points are not clearly distinguishable from the background. This is due mostly to the large variation in background measurements reflecting the instrument limitation in determining low concentration levels.
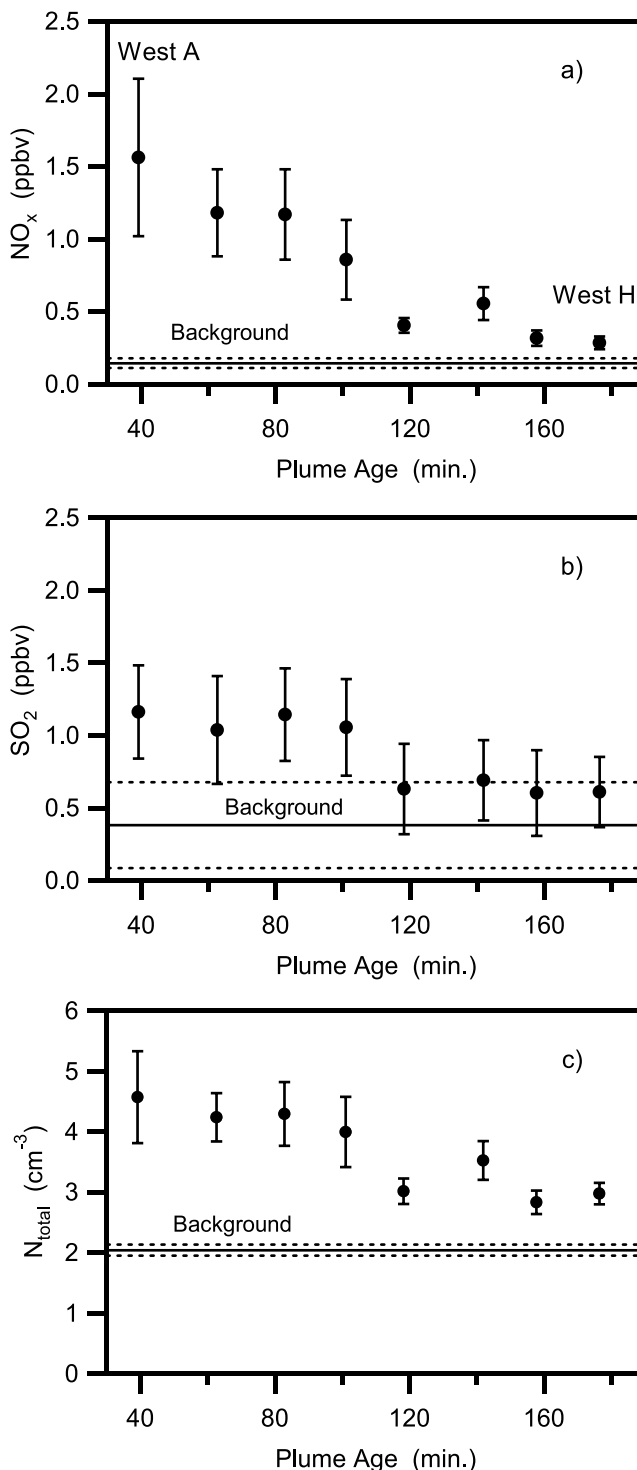
Figure 4. Average values of NO_x, SO_2, and N_{total} as a function of estimated plume age. Symbols and error bars denote averages and standard deviations for plume transects (from left to right) A to H. The solid and dashed lines show the average background levels and associated standard deviations.
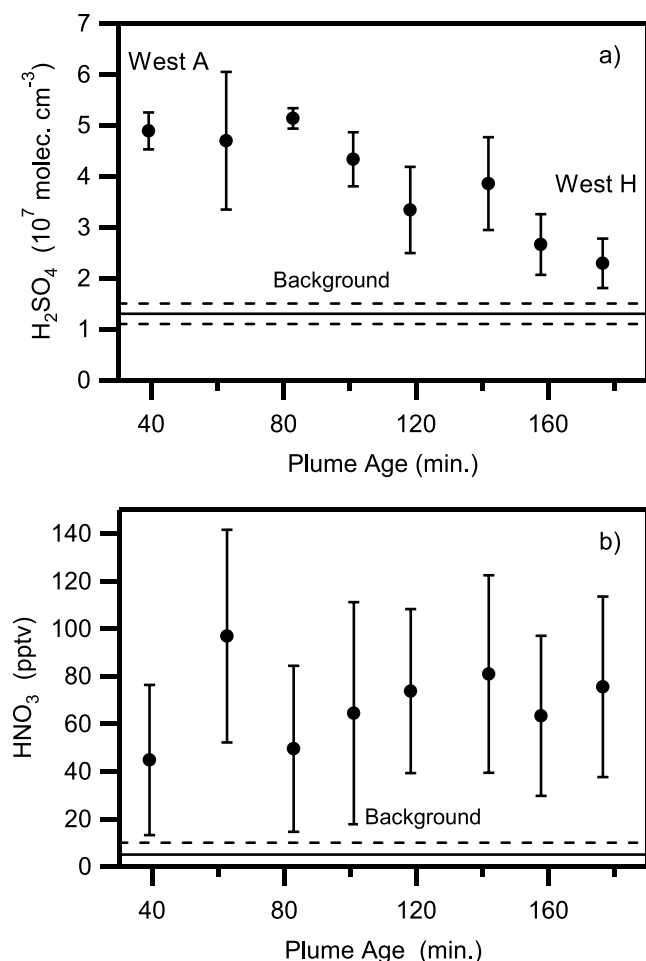
Figure 5. Averages over plume transects of observed (a) H_2SO_4 and (b) HNO_3 as a function of the estimated plume age. Symbols and error bars denote averages and standard deviations for plume transects (from left to right) A to H. The solid and dashed lines show the average background level and associated standard deviations. The HNO_3 background standard deviation calculated from data integrated from 30 s.

[26] The decrease of plume NO_x is due to both plume dispersion and chemical losses. The concentration ratio approach analysis, i.e., equation (1), is applied on data shown on Figure 4 and an effective west plume NO_x lifetime of 109 ± 21 min is derived from a weighted regression analysis. The R^2 value is estimated at 0.86. An identical analysis was also performed on the east plume of unknown origin (ships were not visually observable.). This yielded an observed NO_x lifetime of 113 ± 23 min which indicates the chemistry is similar between the east and west plumes. The NO_x lifetime derived from ITCT observations is close to the minimum of the instantaneous NO_x lifetimes reported by *Song et al.* [2003a]. For this lifetime, 80% of the ΔNO_x (plume average minus background) observed in transect west A would be removed in about 2.5 hours, the time when the west plume reaches west H. The NO_x loss was also evaluated using the mass balance approach of *Ryerson et al.* [1998]. A net NO_x flux (ship NO_x only) is estimated by integrating over the ship plume transected by

WP-3D. These results indicated that the net flux estimated for west H is only about 17% of that of west A. This suggests that about 83% of ship emitted NO_x was removed from the plume which is in excellent agreement with the concentration ratio approach.

[27] Previous studies have suggested that the shortened plume NO_x lifetime is due to elevated OH levels which result from the high levels of plume NO_x. The ITCT OH measurement did not have sufficient time response for measurements in the plume transects so we use H_2SO_4 as a surrogate species to examine the plume HO_x chemistry. This reflects that the source of H_2SO_4 is the OH initiated oxidation of SO_2 and it has a short lifetime (~5 min for the observed surface area of 120 μm^2 cm^{-3}) due to aerosol scavenging. As shown in Figure 5a, plume average H_2SO_4 maximizes at west C, corresponding to a somewhat reduced NO_x level of 1.2 ppbv, while SO_2 levels were nearly constant as shown in Figure 4b. Assuming the observed H_2SO_4 trend was modulated by OH, the peak at west C is qualitatively consistent with previous studies that the highest OH does not correspond to the highest NO_x [e.g., *Song et al.*, 2003a] (see further discussion in section 4.1).

[28] Figure 5b shows the plume average and standard deviation of HNO_3 mixing ratio (filtered by N_{total}) as well as the average background level and its standard deviation. The HNO_3 background levels were generally lower than the 25 pptv precision of the 1 s nitric acid measurement. The average background HNO_3 level was estimated at ~5 pptv ± 5 pptv by averaging 30 s of data before and after each plume. The plume average HNO_3 is significantly higher than the background levels, but is much lower than plume NO_x levels, i.e., 40–100 pptv for HNO_3 versus 280–1600 pptv for NO_x. Either HNO_3 is not efficiently formed by NO_x oxidation in the ship plume, or there is a rapid loss process for HNO_3.

[29] Another way to assess the NO_x to HNO_3 conversion is to examine the relationship between measured NO_x and NO_y. Figure 6 shows the relation between plume averages of NO_x and NO_y, i.e., ΔNO_x and ΔNO_y. The plume averages were normalized by ΔN_{total} to minimize the difference in the impact of plume dispersion on these nitrogen species. As shown in figure, $\Delta NO_x/\Delta N_{total}$ and $\Delta NO_y/\Delta N_{total}$ are strongly correlated with a R^2 value of 0.99 and a slope of 0.86. A nearly identical relationship was also seen in the data collected in the east plume. This indicates that NO_x is the major component of NO_y and there was no significant accumulation of HNO_3 in the plume. Previous studies of intense NO_x sources (e.g., power plant) have shown significant buildup of gas phase HNO_3 and a reduction of the NO_x to NO_y slope to values much less than one [*Ryerson et al.*, 2001; *Neuman et al.*, 2002]. Thus the low in-plume HNO_3 levels, relative to NO_x, suggest that either OH oxidation is not the major NO_x sink or that there is a strong HNO_3 sink. Model simulations that assess the sources and sinks of HNO_3 as well as the in-plume sink of NO_x are discussed in section 4.2.

4. Model Results

[30] In this section, we present the results from the modeling analysis. The gas phase plume chemistry is evaluated in terms of OH levels, NO_x lifetime and oxidation
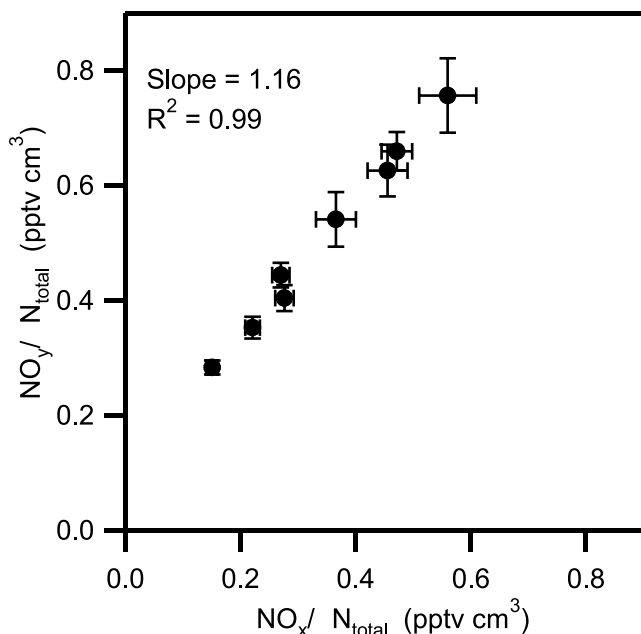
Figure 6. Correlation between the observed plume enhancements NO_y and NO_x normalized to the particle concentration enhancements. Symbols and error bars denote averages and standard deviations of over plume transects (from left to right) A to H.

products. Finally, the interactions between aerosol particles and plume chemistry are assessed.

4.1. OH Levels

[31] The hypothesis of rapid in-plume NO_x loss is based on the prediction of highly elevated OH levels. Figure 7 shows the average plume OH levels from model calculations constrained by observations. These averages are also filtered by N_{total} as previously described. Also shown in the figure are the corresponding observed plume NO_x values and the model calculated background OH level, i.e., OH levels calculated outside of the ship plume. It can be seen that plume OH levels are about a factor of 1.2 to 2.7 higher than background levels. The highest plume OH average of $\sim 1.6 \times 10^7$ molecules cm^{-3} is seen at west D, corresponding to a NO_x level of ~ 0.9 ppbv. It is also clear that plume OH itself varies by nearly a factor of 1.6. This variation is primarily driven by changes in NO_x levels that impact the HO_2 to OH ratio. While the total HO_x (OH + HO_2) level decreases with increasing NO_x level due to the losses from the NO_2 + OH reaction, increasing NO_x also shifts the partitioning in favor of OH via the HO_2 + NO reaction. The model estimated HO_2/OH ratio ranges from 13 for west A, where NO_x is highest, to 57 for west H, where NO_x is lowest. Background ratios are around 90. The overall average plume HO_x level is about a factor of 1.5 lower than the background value, with this ratio ranging from ~ 3 at the high NO_x level at west A to near unity for the lower NO_x at west H. The OH + NO_2 reaction is the predominant HO_x loss within plume, contributing nearly 40% of the total in contrast to only $\sim 1\%$ contribution to the total loss under background conditions. It should also be noted that since the ITCT ship experiment was conducted

around midday local time the primary HO_x production from $O(^1D) + H_2O$ reaction was fairly constant with a variation of less than 15%. Finally, the particle scavenging of HO_2 is estimated to have a 5% or less effect on model OH levels, which is based on estimates using in situ observed particle number/size distributions and an assumption of HO_2 reaction probability of 0.2.

[32] Although observation-constrained model predictions suggest highly elevated OH levels in the ship plume, these predictions must be verified by observations to test the validity of current photochemical theory for ship plumes. For this reason the H_2SO_4 data were used to test model OH predictions. The production of gas phase H_2SO_4 is effectively determined by the SO_2 + OH reaction. The major H_2SO_4 sink is particle scavenging which can be evaluated using the formulation developed by *Fuchs and Sutugin* [1970] and in situ observed number and size distribution data. The value for the sulfuric acid mass accommodation coefficient used in this calculation is 0.7, based on a recent recommendation by *Sander et al.* [2003]. To reduce the uncertainty from large fluctuations due to instrumental noise and ambient variations, both SO_2 and the particle number and size distribution data are averaged for each ship plume transect with the N_{total} filter. The resulting first-order H_2SO_4 scavenging coefficient corresponds to a lifetime of 4.5 to 6 min. Over 95% of the scavenging is attributed to submicron particles as they account for 90% of the total surface area, which averages around 120 μm^2 cm^{-3}. Compared to the background, the in-plume scavenging rate coefficient is about 45% higher. On the basis of the lifetime estimates, we assume steady state for H_2SO_4. The calculated and observed H_2SO_4 are shown in Figure 8. Comparison between observations and model values reveals a high degree of covariation with a R^2 value of 0.9. There is a significant offset of 1×10^7 molecules cm^{-3} and a slope of 2.0. This suggests that model-predicted OH may be low by up to a factor of two. Uncertainty in modeled OH, measured SO_2 and H_2SO_4, and the estimated scavenging rate could all play a role in this discrepancy.
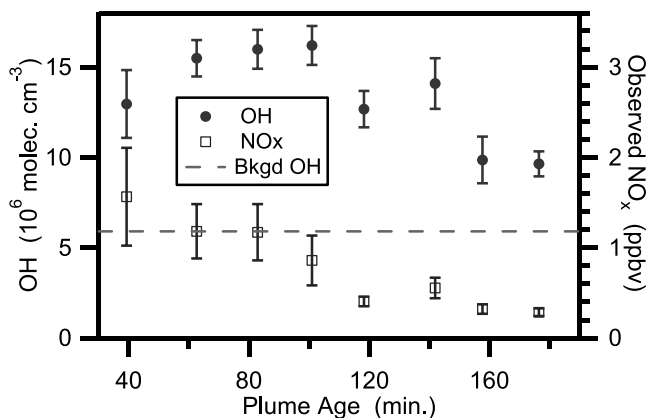
Figure 7. Averages of the model calculated OH (solid circle) and the observed NO_x (open square) as a function of the estimated plume age. The dashed line denotes the background OH level. Averages are made over each of the eight plume transects. Error bars denote the standard deviation calculated for the plume transects.
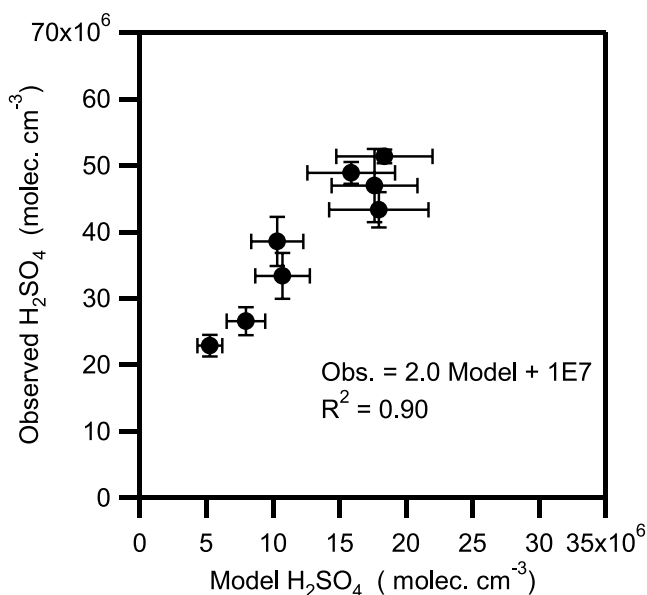
Figure 8. Model-predicted and observed H_2SO_4. Symbols and error bars denote averages and standard deviations for plume transects (from left to right) A to H.

[33] The marine boundary layer of the study has moderately elevated nonmethane hydrocarbon (NMHC) levels. Consequently, the intermediate products of NMHC oxidation (e.g., CH_2O) may be significantly higher than the steady state values calculated from the model [*Fried et al.*, 2003; *Olson et al.*, 2004]. To explore this potential impact on OH, we have carried out sensitivity calculations based on the 95th percentile of CH_2O observation (i.e., ∼900 pptv) made in the MBL during a recent NASA field program TRACE-P. This amount of CH_2O, however, has a less than 5% effect on plume OH levels because HO_x produced from CH_2O photolysis is far smaller than that from $O(^1D) + H_2O$ reaction. Another possible OH source involves heterogeneous reaction between NO_2 and soot to produce nitrous acid (HONO). However, based on a reaction probability of 5×10^{-4} measured by *Longfellow et al.* [1999], we estimate this source is negligible for the conditions encountered in this study.
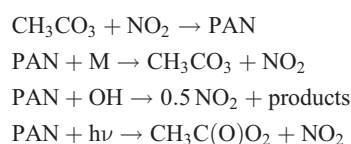
4.2. NOx Lifetime and Oxidation Products

[34] In section 3.2, NO_x lifetimes of 109 ± 21 and 113 ± 23 min were directly estimated from observations for the west and east plumes, respectively. Here we compare the model derived quantities with these values to gain an understanding of the major chemical process responsible for plume NO_x destruction.

4.2.1. NOx Instantaneous Chemical Lifetime

[35] The instantaneous NO_x lifetime for a given transect is defined as the ratio of the total burden over the total loss rate. The quantity can be estimated by calculating the ratio of average NO_x loss rate across the transect to the average NO_x concentration. Figure 9 shows the model estimated NO_x instantaneous lifetime for the west plume transects and corresponding average OH levels as a function of plume age for all 8 plume transects. The NO_x lifetime ranges from 2.5 hours to just over 3 hours, which are substantially

shorter than the background NO_x lifetime of ∼6.5 hour for the time period of the ITCT ship experiment. Similarly, the model NO_x lifetime estimated for the east plume varies from 2.1 to 2.8 hours. The variation of the lifetime is anticorrelated with OH levels. This strong anticorrelation reflects that $OH + NO_2$ is the main NO_x loss process, contributing ∼85 to 90% for west A through D and ∼65 to 75% for the rest of later transects. The other significant ship plume NO_x sink involves formation of PAN. Note that heterogeneous losses of NO_x have been found to be negligibly small. For the ship plume experiment, the PAN lifetime is dominated by thermal decomposition and ranges from 7.5 to 8 hours which is substantially longer than the duration of the experiment itself. Thus production of PAN would be observed as a NO_x loss during the experiment. The PAN reaction sequence is shown below:

$$CH_3CO_3 + NO_2 \rightarrow PAN$$
$$PAN + M \rightarrow CH_3CO_3 + NO_2$$
$$PAN + OH \rightarrow 0.5\,NO_2 + products$$
$$PAN + h\nu \rightarrow CH_3C(O)O_2 + NO_2$$

The net rate of NO_x loss from these processes, $L(NO_x)_{PAN}$, can be estimated by the difference between PAN formation rate and the NO_x feedback from PAN, i.e.,

$$L(NO_x)_{PAN} = k_1[CH_3CO_3][NO_2] - (k_2 + 0.5k_3[OH] + j_4)[PAN]_{obs}$$

(2)

where k_1, k_2, k_3 and j_4 are rate coefficients for reactions 1 to 4, respectively.
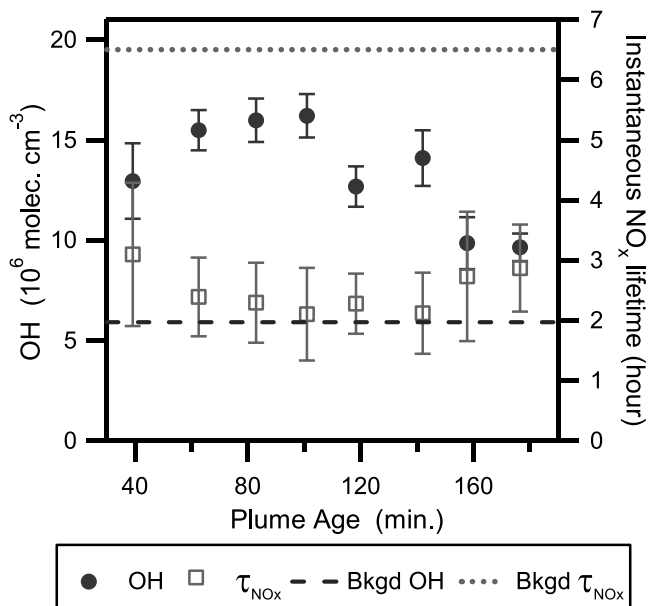
Figure 9. Averages of the model calculated OH (solid circles) and the model-predicted instantaneous NO_x lifetime (open squares) as a function of the estimated plume age. Averages are made over each of the eight plume transects. Error bars denote the standard deviation calculated for the plume transects.

[36] The rate of PAN formation can be predicted by a model based on the observed values of precursors; while the rate of feedback to NO_x is estimated using observed PAN values together with model calculated OH and j_4 as well as reaction rate coefficients from *DeMore et al.* [1997]. It should be noted that there are very limited PAN observations available in and around the west plume during the experiment. The available observations suggest that there is no statistically significant difference in PAN between earlier transects and later transects and the difference between inside and outside of the plume is also indistinguishable. Thus we have used the average of 135 pptv for $[PAN]_{obs}$ in equation (2). We predict a 60 pptv PAN increase from west A to west H assuming PAN concentration is at background level at west A. This increase is about 3 times higher than the reported measurement precision [*Roberts et al.*, 2004] and should be detectable. The absence of any observed change in PAN may be attributed to several factors, including the limited number of in situ observations (i.e., 5 measurements near the fringe of the plume and 1 close to the center of the plume), kinetic coefficients, and the uncertainty in model prediction of $CH_3C(O)O_2$, which may be considerably larger than that of OH due to the uncertainties in NMHC oxidation mechanism.

4.2.2. Equivalent NO_x Chemical Lifetime

[37] The instantaneous lifetime represents the rate of NO_x decay at a particular point in time. The concept of equivalent lifetime is used here to address the average loss rate of NO_x over the 2.5 hour of processing observed for the ITCT ship plume. The instantaneous NO_x chemical lifetime is a function of plume age as shown in Figure 9. The working definition of equivalent NO_x chemical lifetime is the time required to reproduce the NO_x decrease (defined by the ratio of starting and ending concentrations) for a given time period under the assumption of exponential decay. On the basis of this definition, the equivalent lifetime can be derived from instantaneous lifetime using the equation below:

$$\tau_{eqv} = \frac{\Delta t}{\int_t^{t+\Delta t} \frac{1}{\tau_{inst}} dt'} \tag{3}$$

where τ_{eqv} and τ_{inst} are the equivalent NO_x and instantaneous NO_x chemical lifetimes, respectively; and Δt is the time period of interest. From the lifetime values shown in Figure 9, a model equivalent lifetime is calculated to be 143 ± 40 min. For the east plume, the estimated equivalent lifetime is 135 ± 37 min. The uncertainty cited can be attributed to those in model calculations, e.g., OH and $CH_3C(O)O_2$. If only OH oxidation were considered, the τ_{eqv} value would be 172 ± 45 min. Comparing to the observed τ_{eqv} of 109 ± 21 min, the model τ_{eqv} is significantly longer even though the uncertainties overlap each other. This may suggest that the model OH could be underestimated by about 30%, which is qualitatively consistent with the suggestion of low model-predicted OH determination from the H_2SO_4 analysis. More importantly, both observed and model τ_{eqv} values are much smaller than the calculated background NO_x lifetime of ~6.5 hours for the time period of the ITCT ship

experiment (Note: the diurnal average NO_x lifetime is estimated to be 21 hours for the background conditions). Finally, we would like to point out another source of this difference between model and observations. The model τ_{eqv} is defined to reproduce the difference between the NO_x levels at the start point and end point of the time period of interest. The observed τ_{eqv}, however, represents the average rate of the NO_x decay, as it is derived from regression analysis. If only the data from west A and west H (start and end points) were used, the resulting τ_{eqv} would be 127 ± 21 min, which is closer to the model value.

4.2.3. HNO_3

[38] In the past two sections, we have shown that ship plume NO_x lifetime is considerably shorter than for the unperturbed marine boundary layer. This short lifetime is believed to be primarily due to a large enhancement in OH levels. Thus one would expect that the plume has much higher HNO_3 concentrations than background. The photochemical model predicts that around 300–400 pptv of HNO_3 should have been observed from west C to west H transects. This prediction is under the assumption that the major sinks of plume HNO_3 are plume dispersion and dry deposition with a velocity of ~0.6 cm sec^{-1} for the wind speed observed during the ITCT ship experiment [*Pryor and Sorensen*, 2000]. The boundary layer depth used here is 300 m.

[39] The observed HNO_3 mixing ratios range from 40 to 100 pptv with an average of 69 pptv (Figure 5b). The low HNO_3 values are consistent with the observed relation between NO_x and NO_y (see section 3.2). However, model to measurement comparison of H_2SO_4 suggests model-predicted OH levels may be as much as a factor of 2 too low. The model also under estimates the observed τ_{eqv} by at least 30%. Consequently, the model does not likely over-estimate the rate of NO_x oxidation by OH which leads to HNO_3 formation. Thus additional or stronger sinks are needed to reconcile the difference between model and observed HNO_3. An average HNO_3 lifetime of ~20 min would reconcile the model predictions with average observations calculated from the west A to west H transects. This lifetime is nearly a factor of six shorter than the current lifetime based on plume dispersion and dry deposition. If there were no additional sinks, the dry deposition velocity would have to be ~25 cm sec^{-1}, more than one order of magnitude higher than literature reported values. This rapid HNO_3 loss is not unique to this experiment. Similar rates of HNO_3 loss were also observed in power plant and refinery plumes during TexAQS 2000, which could not be explained by known sinks [*Neuman et al.*, 2003]. Another potential sink is particle scavenging of HNO_3. On the basis of the observed aerosol number size distribution, it would require a reaction probability, γ, of 0.12. This value is at, if not above, the upper limit of current literature reported value. The average observed total particle surface area for the plume transects was ~120 μm^2 cm^{-3} and the average for the background was 90 μm^2 cm^{-3}. This difference can mostly be attributed to the particle size range under 150 nm. The scavenging due to this size range is estimated to be ~45% of the total for the plume transects and ~29% for the background conditions. Considering the high wind speed of
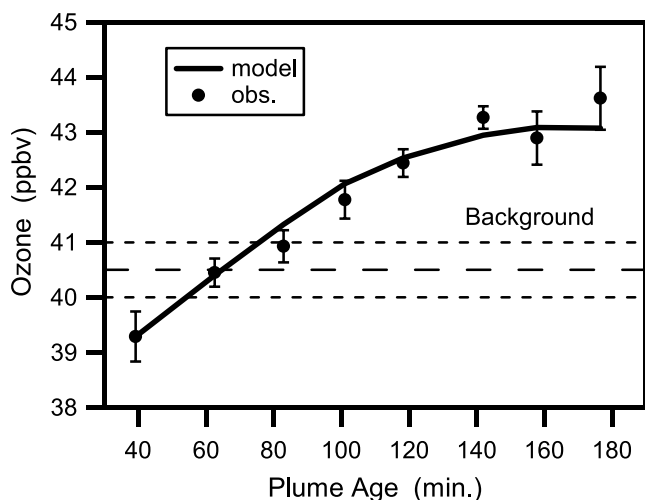
Figure 10. Averages of observed (solid circle) and model-predicted (solid line) ozone versus estimated plume age. Averages are made over each of the 8 plume transects. Error bars represent the standard deviations. The long and short dashed lines show the average background ozone levels and the standard deviations.

9–11 m s^{-1}, it is not unreasonable to assume that background particles larger than 150 nm are mostly sea salt. This assumption is, at least partially, based on reported observations of significant portion of submicron sea-salt particles down to as low as ~200 nm [*Murphy et al.*, 1998; *Wang et al.*, 2002]. In this context, one would conclude that sea-salt scavenging was the major sink of HNO$_3$ while the contribution from ship emitted particles remains significant.

[40] It should be noted that thermodynamic models cannot be used to predict the partitioning between gas phase HNO$_3$ and particulate NO$_3^-$ because there are no data on either NH$_3$ or NH$_4^+$ available for the experiment. The few available PILS submicron plume NO$_3^-$ measurements show no significant difference between the inside and outside of plume; while we predict more than a factor of ~5 increase in particulate NO$_3^-$ would be observed in transect H if HNO$_3$ were lost to particles. However, it should also be recognized that the PILS would not be able to observe a significant nitrate increase if most submicron nitrate was in organic forms. The total particle volume increase is estimated at 1 ± 0.4 μm^3 cm^{-3} from uptake of gas phase HNO$_3$ and H$_2$SO$_4$. This value is estimated using a γ value of 0.1 for HNO$_3$ and a sticking coefficient of 0.7 for H$_2$SO$_4$ together with observed gas phase concentrations. Comparing to average observed plume particle volume of ~8 μm^3 cm^{-3}, this growth is relatively minor and not likely to be observed given the instrument precision and natural fluctuations. Another possibility for the rapid loss of HNO$_3$ is efficient uptake on larger sea salt aerosol which is expected to have diameters typically greater than 1 μm [*Seinfeld and Pandis*, 1998]. However, there is not enough observed surface area in this size range to account for the HNO$_3$ loss even at a diffusion limited rate. While we cannot draw more definitive conclusions about the contribution of particle scavenging to a HNO$_3$ loss because of the limited availability of data, this analysis serves to further constrain the magnitude of additional HNO$_3$ losses necessary to explain observations within pollution plumes.

4.3. Ozone Production

[41] We have estimated ship plume ozone evolution based on the following equation:

$$\frac{d[O_3]_{plm}}{dt} = P(O_3) - L_{photo}[O_3]_{plm} + L_{disp}\left([O_3]_{bkg} - [O_3]_{plm}\right) \quad (4)$$

where $[O_3]_{plm}$ and $[O_3]_{bkg}$ are ozone concentrations of plume and background, respectively; $P(O_3)$ is photochemical ozone production; L_{photo} is the photochemical ozone loss frequency; and L_{disp} is the loss frequency due to plume dispersion. The values of $P(O_3)$ and L_{photo} are calculated by the model and the value of L_{disp} is estimated from the decay of ΔN_{total} (see section 3.1). Figure 10 displays the comparison of the model simulated and observed ozone as well as the background ozone value. The model calculation is initialized by the average of ozone observed in west A. As shown in the figure, the model captures the observed trend and the model bias is less than 5%. This good agreement can be viewed as an indirect confirmation of model-predicted peroxy radicals, mostly HO$_2$. Although the west A ozone concentration is lower than the background level, model calculations indicate photochemistry is a net source of ozone at a rate of 2.3 ppbv hour^{-1}. The initial ozone concentration is lower than background due to titration by emitted NO as evidenced by the highly elevated NO$_x$ prior to west A. Even higher net ozone production is estimated for west B, C, and D ~2.9 ppbv hour^{-1}. For west H, this rate decreases to 0.9 ppbv hour^{-1}.

[42] The ozone production efficiency, defined as the ratio of ozone produced to NO$_x$ consumed, ranges from 6 for west A to 30 for west H with an average value of 10 and is anticorrelated with the NO$_x$ level. This average value agrees well with that derived from a regression analysis between ozone and the amount of NO$_x$ removed. The total ozone production for the sampling period is 4.0 ppbv and a net increase of 2.5 ppbv over the background. The largest production channel is HO$_2$ + NO which contributes ~76%; while the major ozone sinks involves two sequences of reactions: (1) ozone photolysis followed by reaction of O(^{1}D) + H$_2$O and (2) O$_3$ + NO followed by NO$_2$ + OH. The former dominates in lower NO$_x$ transects, i.e., west E through west H, contributing over 50%; while the second sequence accounts for 40–50% of the total ozone loss for west A through west C.

5. Conclusions

[43] The observations demonstrate rapid plume NO$_x$ loss, i.e., ~80% of ship emitted NO$_x$ was removed within the duration of the experiment ~2.5 hours. The equivalent ship plume lifetime derived from the observed NO$_x$ decay is ~1.8 hours. By contrast, the model estimated NO$_x$ lifetime in the background marine boundary layer is 6.5 hours for midday conditions. The model-predicted plume NO$_x$ lifetime is 2.4 hours, about 30% higher than that derived from observations. The model analysis primarily attributes this rapid NO$_x$ loss to oxidation by elevated plume OH levels.

Formation of PAN is estimated to also have significant contribution as a temporary sink of plume NO_x. However, PAN is a reservoir of NO_x that may further extend the influence of ship plumes to the remote marine atmosphere. It should be noted that the estimate of net plume NO_x loss through PAN is based on limited in-plume observations, which may not be representative of the whole plume and there is little experimental evidence for enhanced PAN production in the plumes. Fast PAN measurements would be desirable in future experiments to further elucidate and quantify the role of PAN.

[44] To test our understanding of ship plume chemistry, model/measurement comparisons of H_2SO_4 and O_3 were conducted as indirect tests of OH and HO_2, respectively. Comparison of H_2SO_4 showed that the model prediction is highly correlated with the observations with a R^2 value of 0.9, but model values are significantly lower than the observations. An increase of model OH by a factor of 2 would remove the discrepancy. The model underestimated the observed rate of NO_x loss by about 30%, which also suggests model OH estimates may be lower than the actual ambient values; although this difference is well within the estimated uncertainties for model and observations. However, if the model predictions of PAN formation are in error the discrepancy is even larger. The model simulation of plume ozone is within 10% of the observations. This suggests that the model-predicted HO_2 is quite reasonable. Of course, a more conclusive test would involve in-plume measurements of both OH and HO_2.

[45] The largest model disagreement was with the observed levels of HNO_3 in the ship plumes. The observed plume level varies from 40 to 100 pptv, with an average of 69 pptv. Model calculations predict plume HNO_3 levels ranging from ~300 to 400 pptv. We believe that the model over-estimation is caused by a missing or under-estimated sink for HNO_3. To reproduce the average observation, an average HNO_3 lifetime of ~20 min is required. One potential process that can account for this rapid loss is particle scavenging with assumptions of irreversible loss and reaction probability of >0.1. However, the time resolution of particulate nitrate measurements could not provide a clear indication of in-plume nitrate increase. The lack of NH_4^+ measurements prevented a test to check if the thermodynamic equilibrium would allow uptake of HNO_3. On the basis of estimates of gas phase uptake of HNO_3 and H_2SO_4, the total particle volume would have increased by 1 μm^3 cm^{-3}, or 12%. This increase is significant, but smaller than the combined uncertainty due to measurement precision and atmospheric variability. We believe this is a critical issue that should be addressed in the future. Fast and accurate observations of particle chemical composition (including organic nitrate) would be required to address this problem.

[46] Ship emission factors are derived from observations for NO_x, SO_2, and total particle concentration. While good agreement with previously reported values are obtained for NO_x and total particle concentration, the values for SO_2 emission factor appears to be a factor of 1.6 to 1.9 lower than literature values which are generally consistent (i.e., within 25%) with the values derived from the fuel sulfur content aboard the identified ship. This suggests that the sulfur chemistry in this experiment occurs at significantly lower levels than expected for more typical ship emissions.

References

Beirle, S., U. Platt, R. von Glasow, M. Wenig, and T. Wagner (2004), Estimate of nitrogen oxide emissions from shipping by satellite remote sensing, *Geophys. Res. Lett.*, *31*, L18102, doi:10.1029/2004GL020312.

Blake, N. J., et al. (1999), Influence of southern hemispheric biomass burning on midtropospheric distributions of nonmethane hydrocarbons and selected halocarbons over the remote South Pacific, *J. Geophys. Res.*, *104*(D13), 16,213–16,232.

Brock, C. A., F. Schroder, B. Karcher, A. Petzold, R. Busen, and M. Fiebig (2000), Ultrafine particle distributions measured in aircraft exhaust plumes, *J. Geophys. Res.*, *105*(D21), 26,555–26,567.

Brock, C. A., et al. (2003), Particle growth in urban and industrial plumes in Texas, *J. Geophys. Res.*, *108*(D3), 4111, doi:10.1029/2002JD002746.

Brock, C. A., et al. (2004), Chemical and microphysical characteristics of aerosols in the free troposphere near the west coast of North America, *J. Geophys. Res.*, *109*, D23S26, doi:10.1029/2003JD004198.

Capaldo, K., J. J. Corbett, P. Kasibhatla, and S. N. Pandis (1999), Effects of ship emissions on sulphur cycling and radiative climate forcing over the ocean, *Nature*, *400*, 743–746.

Chen, G., D. D. Davis, P. Kasibhatla, A. R. Bandy, D. C. Thornton, B. J. Huebert, A. D. Clarke, and B. W. Blomquist (2000), A study of DMS oxidation in the tropics: Comparison of Christmas Island field observations of DMS, SO2, and DMSO with model simulations, *J. Atmos. Chem.*, *37*(2), 137–160.

Corbett, J. J. (2003), New directions: Designing ship emissions and impacts research to inform both science and policy, *Atmos. Environ.*, *37*(33), 4719–4721.

Corbett, J. J., and H. W. Koehler (2003), Updated emissions from ocean shipping, *J. Geophys. Res.*, *108*(D20), 4650, doi:10.1029/2003JD003751.

Corbett, J. J., P. S. Fischbeck, and S. N. Pandis (1999), Global nitrogen and sulfur inventories for ocean-going ships, *J. Geophys. Res.*, *104*, 3457–3470.

Crawford, J., et al. (1999), Assessment of upper tropospheric HOx sources over the tropical Pacific based on NASA GTE/PEM data: Net effect on HOx and other photochemical parameters, *J. Geophys. Res.*, *104*(D13), 16,255–16,273.

Davis, D. D., et al. (1996), Assessment of ozone photochemistry in the western North Pacific as inferred from PEM-West A observations during the fall 1991, *J. Geophys. Res.*, *101*(D1), 2111–2134.

Davis, D. D., G. Grodzinsky, P. Kasibhatla, J. Crawford, G. Chen, S. Liu, A. Bancy, D. Thornton, H. Guan, and S. Sandholm (2001), Impact of ship emissions on marine boundary layer NO_x and SO_2 distributions over the Pacific Basin, *Geophys. Res. Lett.*, *28*(2), 235–238.

DeMore, W. B., et al. (1997), Chemical kinetics and photochemical data for use in stratospheric modeling: Evaluation number 12, *JPL Publ. 97-4*, NASA Jet Propul. Lab., Pasadena, Calif.

Durkee, P. A., K. J. Noone, and R. T. Bluth (2000a), The Monterey Area Ship Track experiment, *J. Atmos. Sci.*, *57*(16), 2523–2541.

Durkee, P. A., R. E. Chartier, A. Brown, E. J. Trehubenko, S. D. Rogerson, C. Skupniewicz, K. E. Nielsen, S. Platnick, and M. D. King (2000b), Composite ship track characteristics, *J. Atmos. Sci.*, *57*(16), 2542–2553.

Eisele, F. L., and D. J. Tanner (1993), Measurement of the gas-phase concentration of H_2SO_4 and methane sulfonic-acid and estimates of H_2SO_4 production and loss in the atmosphere, *J. Geophys. Res.*, *98*(D5), 9001–9010.

Eisele, F. L., R. L. Mauldin, D. J. Tanner, J. R. Fox, T. Mouch, and T. Scully (1997), An inlet/sampling duct for airborne OH and sulfuric acid measurements, *J. Geophys. Res.*, *102*, 27,993–28,001.

Endresen, Ø., E. Sørgård, J. K. Sundet, S. B. Dalsøren, I. S. A. Isaksen, T. F. Berglen, and G. Gravir (2003), Emission from international sea transportation and environmental impact, *J. Geophys. Res.*, *108*(D17), 4560, doi:10.1029/2002JD002898.

European Commission and ENTEC UK Limited (2002), Quantification of emissions from ships associated with ship movements between ports in the European Community, Eur. Commiss., Brussels.

Ferek, R. J., D. A. Hegg, P. V. Hobbs, P. Durkee, and K. Nielsen (1998), Measurements of ship-induced tracks in clouds off the Washington coast, *J. Geophys. Res.*, *103*(D18), 23,199–23,206.

Fried, A., et al. (2003), Airborne tunable diode laser measurements of formaldehyde during TRACE-P: Distributions and box model comparisons, *J. Geophys. Res.*, *108*(D20), 8798, doi:10.1029/2003JD003451.

Frost, G. J., et al. (1999), Photochemical modeling of OH levels during the first aerosol characterization experiment (ACE 1), *J. Geophys. Res.*, *104*(D13), 16,041–16,052.

Frost, G. J., et al. (2002), Comparisons of box model calculations and measurements of formaldehyde from the 1997 North Atlantic Regional Experiment, *J. Geophys. Res.*, *107*(D8), 4060, doi:10.1029/2001JD000896.

Fuchs, N. A., and A. G. Sutugin (1970), *Highly Dispersed Aerosols*, Ann Arbor Sci. Publ., Ann Arbor, Mich.

Hanna, S. R., L. L. Schulman, R. J. Paine, J. Pleim, and M. Baer (1985), Development and evaluation of the offshore and coastal dispersion model, *J. Air Pollut. Control Assoc.*, *35*, 1039–1047.

Heidt, L. E., J. F. Vedder, W. H. Pollock, R. A. Lueb, and B. E. Henry (1989), Trace gases in the Antarctic atmosphere, *J. Geophys. Res.*, *94*, 11,599–11,611.

Hobbs, P. V., et al. (2000), Emissions from ships with respect to their effects on clouds, *J. Atmos. Sci.*, *57*, 2570–2590.

Holloway, J. S. R. O. Jakoubek, D. D. Parrish, C. Gerbig, A. Volz-Thomas, S. Schmitgen, A. Fried, B. Wert, B. Henry, and J. R. Drummond (2000), Airborne intercomparison of vacuum ultraviolet fluorescence and tunable diode laser absorption measurements of tropospheric carbon monoxide, *J. Geophys. Res.*, *105*, 24,251–24,261.

International Maritime Organization and Marine Environment Protection Committee (2001), Prevention of air pollution from ships—Sulfur monitoring 2000, Int. Maritime Org., London.

Kasibhatla, P., et al. (2000), Do emissions from ships have a significant impact on concentrations of nitrogen oxides in the marine boundary layer?, *Geophys. Res. Lett.*, *27*, 2229–2232.

Lawrence, M. G., and P. J. Crutzen (1999), Influence of NO$_x$ emissions from ships on tropospheric photochemistry and climate, *Nature*, *402*, 167–170.

Lee, D. S., I. Köhler, E. Grobler, F. Rohrer, R. Sausen, L. Gallardo-Klenner, J. J. G. Olivier, F. J. Dentener, and A. F. Bouwman (1997), Estimates of global NO$_x$ emissions and their uncertainties, *Atmos. Environ.*, *31*, 1735–1749.

Logan, J. A., M. J. Prather, S. C. Wofsy, and M. B. McElroy (1981), Tropospheric chemistry—A global perspective, *J. Geophys. Res.*, *86*, 7210–7254.

Longfellow, C. A., A. R. Ravishankara, and D. R. Hanson (1999), Reactive uptake on hydrocarbon soot: Focus on NO$_2$, *J. Geophys. Res.*, *104*, 13,833–13,840.

Lurmann, F. W., A. C. Lloyd, and R. Atkinson (1986), A chemical mechanism for use in long-range transport/acid deposition computer modeling, *J. Geophys. Res.*, *91*, 10,905–10,936.

Lyyränen, J., J. Jokiniemi, E. I. Kauppinen, and J. Joutsensaari (1999), Aerosol characterisation in medium-speed diesel engines operating with heavy fuel oils, *J. Aerosol Sci.*, *30*, 771–784.

Mauldin, R. L., D. J. Tanner, J. A. Heath, B. J. Huebert, and F. L. Eisele (1999a), Observations of H2SO4 and MSA during PEM-Tropics-A, *J. Geophys. Res.*, *104*(D5), 5801–5816.

Mauldin, R. L., D. J. Tanner, and F. L. Eisele (1999b), Measurements of OH during PEM-Tropics A, *J. Geophys. Res.*, *104*(D5), 5817–5827.

Murphy, D. M., D. S. Thomson, A. M. Middlebrook, and M. E. Schein (1998), In situ single-particle characterization at Cape Grim, *J. Geophys. Res.*, *103*(D13), 16,485–16,491.

Neuman, J. A., et al. (2002), Fast-response airborne in situ measurements of HNO$_3$ during the Texas 2000 Air Quality Study, *J. Geophys. Res.*, *107*(D20), 4436, doi:10.1029/2001JD001437.

Neuman, J. A., et al. (2003), Variability in ammonium nitrate formation and nitric acid depletion with altitude and location over California, *J. Geophys. Res.*, *108*(D17), 4557, doi:10.1029/2003JD003616.

Nicks, D. K., et al. (2003), Fossil-fueled power plants as a source of atmospheric carbon monoxide, *J. Environ. Monit.*, *5*(1), 35–39.

Noone, K. J., et al. (2000), A case study of ships forming and not forming tracks in moderately polluted clouds, *J. Atmos. Sci.*, *57*(16), 2729–2747.

Nowak, J. B., et al. (2004), Gas-phase chemical characteristics of Asian emission plumes observed during ITCT 2K2 over the eastern North Pacific Ocean, *J. Geophys. Res.*, *109*, D23S19, doi:10.1029/2003JD004488.

Olson, J. R., et al. (2001), Seasonal differences in the photochemistry of the South Pacific: A comparison of observations and model results from PEM-Tropics A and B, *J. Geophys. Res.*, *106*, 32,749–32,766.

Olson, J. R., et al. (2004), Testing fast photochemical theory during TRACE-P based on measurements of OH, HO$_2$, and CH$_2$O, *J. Geophys. Res.*, *109*, D15S10, doi:10.1029/2003JD004278.

Orsini, D. A., Y. Ma, A. Sullivan, B. Sierau, K. Baumann, and R. J. Weber (2003), Refinements to the particle-into-liquid-sampler (PILS) for ground and airborne measurements of water-soluble aerosol composition, *Atmos. Environ.*, *27*, 1243–1259.

Parrish, D. D., Y. Kondo, O. R. Cooper, C. A. Brock, D. A. Jaffe, M. Trainer, T. Ogawa, G. Hübler, and F. C. Fehsenfeld (2004), Intercontinental Transport and Chemical Transformation 2002 (ITCT 2K2) and Pacific Exploration of Asian Continental Emission (PEACE) experiments: An overview of the 2002 winter and spring intensives, *J. Geophys. Res.*, *109*, D23S01, doi:10.1029/2004JD004980.

Pryor, S. C., and L. L. Sorensen (2000), Nitric acid-sea salt reactions: Implications for nitrogen deposition to water surfaces, *J. Appl. Meteorol.*, *39*, 725–731.

Radke, L. F., J. A. Coakley, and M. D. King (1989), Direct and remote-sensing observations of the effects of ships on clouds, *Science*, *246*(4934), 1146–1149.

Roberts, J. M., et al. (2004), Measurement of peroxycarboxylic nitric anhydrides (PANs) during the ITCT 2K2 aircraft intensive experiment, *J. Geophys. Res.*, *109*, D23S21, doi:10.1029/2004JD004960.

Ryerson, T. B., et al. (1998), Emissions lifetime and ozone formation in power plant plumes, *J. Geophys. Res.*, *103*, 22,569–22,583.

Ryerson, T. B., et al. (2001), Observations of ozone formation in power plant plumes and implications for ozone control strategies, *Science*, *292*, 719–723.

Sander, S. P., et al. (2003), Chemical kinetics and photochemical data for use in stratospheric modeling: Supplement to evaluation 14, update of key reactions, *JPL Publ. 02-25*, Jet Propul. Lab., Pasadena, Calif.

Schauffler, S., E. Atlas, D. Blake, F. Flocke, R. A. Lueb, J. Lee-Taylor, V. Stroud, and W. Travnicek (1999), Distributions of brominated organic compounds in the troposphere and lower stratosphere, *J. Geophys. Res.*, *104*, 21,513–21,535.

Seinfeld, J. H., and S. N. Pandis (1998), *Atmospheric Chemistry and Physics—From Air Pollution to Climate Change*, John Wiley, Hoboken, N. J.

Shetter, R. E., et al. (2003), Photolysis frequency of NO$_2$: Measurement and modeling during the International Photolysis Frequency Measurement and Modeling Intercomparison (IPMMI), *J. Geophys. Res.*, *108*(D16), 8544, doi:10.1029/2002JD002932.

Sinha, P., P. V. Hobbs, R. J. Yokelson, T. J. Christian, T. W. Kirchstetter, and R. Bruintjes (2003), Emissions of trace gases and particles from two ships in the southern Atlantic Ocean, *Atmos. Environ.*, *37*, 2139–2148.

Skjølsvik, K. O., A. B. Andersen, J. J. Corbett, and J. M. Skjelvik (2000), Study of greenhouse gas emissions from ships: Report to International Maritime Organization on the outcome of the IMO Study on Greenhouse Gas Emissions from Ships, *Rep. MEPC 45/8*, MARINTEK Sintef Group, Trondheim, Norway.

Smyth, S., et al. (1996), Comparison of free tropospheric western Pacific air mass classification schemes for the PEM-West A experiment, *J. Geophys. Res.*, *101*(D1), 1743–1762.

Song, C. H., G. Chen, S. R. Hanna, J. Crawford, and D. D. Davis (2003a), Dispersion and chemical evolution of ship plumes in the marine boundary layer: Investigation of O$_3$/NO$_y$/HO$_x$ chemistry, *J. Geophys. Res.*, *108*(D4), 4143, doi:10.1029/2002JD002216.

Song, C. H., G. Chen, and D. D. Davis (2003b), Chemical evolution and dispersion of ship plumes in the remote marine boundary layer: Investigation of sulfur chemistry, *Atmos. Environ.*, *37*(19), 2663–2679.

Starcrest Consulting Group LLC, B. Anderson, J. Ray, S. Wells, and G. Aldrete (2004), *The Port of Los Angeles: Revised Draft 2001, Baseline Emissions Inventory*, edited by C. Patton et al., 218 pp., Los Angeles, Calif.

Tuttle, K. L. (1995), Combustion-generated emissions in marine propulsion systems, in *Proceedings of the SNAME 1994 Environmental Symposium—Ship Design and Operation in Harmony with the Environment*, pp. 311–323, Soc. of Nav. Archit. and Mar. Eng., Jersey City, N. J.

Twomey, S. (1977), Influence of pollution on shortwave albedo of clouds, *J. Atmos. Sci.*, *34*(7), 1149–1152.

von Glasow, V., M. Lawrence, R. Sander, and P. J. Crutzen (2003), Modeling the chemical effects of ship exhaust in the cloud-free marine boundary layer, *Atmos. Phys. Chem.*, *3*, 233–250.

Wang, J., et al. (2002), Clear-column radiative closure during ACE-Asia: Comparison of multiwavelength extinction derived from particle size and composition with results from Sun photometry, *J. Geophys. Res.*, *107*(D23), 4688, doi:10.1029/2002JD002465.

Weber, R. J., D. Orsini, Y. Daun, Y.-N. Lee, P. Klotz, and F. Brechtel (2001), A particle-in-liquid collector for rapid measurement of aerosol chemical composition, *Aerosol Sci. Technol.*, *35*, 718–727.

Wilson, J. C., B. G. Lafleur, H. Hilbert, W. R. Seebaugh, J. Fox, D. W. Gesler, C. A. Brock, B. J. Huebert, and J. Mullen (2004), Function and

performance of a low turbulence inlet for sampling super-micron particles from aircraft platforms, *Aerosol Sci. Technol.*, *38*(8), 790–802.

_____

E. Atlas, Division of Marine and Atmospheric Chemistry, Rosenstiel School of Marine and Atmospheric Science, University of Miami, 4600 Rickenbacker Causeway, Miami, FL 33149, USA.

C. Brock, F. Fehsenfeld, J. Holloway, G. Hübler, J. A. Neuman, J. Nowak, D. Parrish, J. Roberts, T. Ryerson, and M. Trainer, NOAA Aeronomy Laboratory, 325 Broadway, R/AL-7, Boulder, CO 80305, USA.

G. Chen, J. Crawford, and J. R. Olson, NASA Langley Research Center, Mail Stop 401B, Hampton, VA 23681, USA. (g.chen@larc.nasa.gov)

J. Corbett, Marine Policy Program, Graduate College of Marine Studies, University of Delaware, 305 Robinson Hall, Newark, DE 19716, USA.

S. Donnelly, Department of Chemistry, Fort Hays State University, Hays, KS 67601, USA.

F. Flocke and S. Schauffler, Atmospheric Chemistry Division, National Center for Atmospheric Research, 1850 Table Mesa Drive, Boulder, CO 80305, USA.

L. G. Huey, A. Sullivan, D. Tanner, and R. Weber, School of Earth and Atmospheric Sciences, Georgia Institute of Technology, 311 Ferst Drive, Atlanta, GA 30332, USA.

D. Nicks, Ball Aerospace, Boulder, CO 80306, USA.